Probabilistic predictions regarding key blocks using stochastic discrete fracture networks – example from a rock cavern in south-east Sweden

P. Starzec · J. Andersson

Abstract The natural variation of the fracture/joint network geometry and limited data access are the main sources of uncertainties in key block predictions. To make the uncertainties easily quantifiable the predicting variables should be presented as probability density functions. This paper illustrates the implementation of a stochastic discrete fracture network to predict the amount and size of key blocks around the rock cavern of the Centralt Storage Facility for Spent Nuclear Fuel (CLAB-2, Central Lager Använt Bränsle) in south-eastern Sweden. The data used in the study were effectively limited to fracture mapping in boreholes. The stochastic fracture model was generated with a FracMan discrete fracture simulator by adopting random fracture locations. Subsequently, the key block statistics along a simulated tunnel positioned inside the fracture model were generated. To illustrate the value of the predictions made, block statistics were undertaken for two different tunnel orientations. The methodology presented offers the potential to optimize the excavation design.

Résumé La variabilité naturelle de la géométrie des réseaux de fractures et l'accès limité aux données sont les principales sources d'incertitudes dans l'identification des blocs clés. Afin de rendre ces incertitudes aisément quantifiables, les paramètres du modèle devraient être représentés par des variables aléatoires. Cet article illustre la simulation d'un réseau stochastique de fractures destiné à prévoir le nombre et la taille des blocs clés autour de la cavité souterraine de l'installation CLAB-2 dans le sud-ouest de la Suède. Les données utilisées dans l'étude furent effectivement limitées à des données de fractures en sondage. Le modèle stochastique de fractures a été obtenu à partir du simulateur FracMan en générant une localisation aléatoire des fractures. Par la suite les données statistiques relatives aux blocs clés le long d'un tunnel fictif placé à l'intérieur du modèle de fractures ont été obtenues. Pour illustrer la valeur des prévisions faites, les données statistiques sur les blocs clés ont été recherchées pour deux orientations de tunnel. La méthodologie présentée permet d'optimiser la conception des cavités souterraines.

Keywords Discrete fracture network · Key blocks · Predictions

Mots clés Réseau de fractures · Blocs clés · Prévisions

Received: 28 November 2000 / Accepted: 22 December 2001
Published online: 13 April 2002

P. Starzec (✉)
Swedish Geotechnical Institute, 412 96 Göteborg, Sweden
e-mail: peter.starzec@swedgeo.se
Tel.: +46-31-7786572
Fax: +46-31-7786575

P. Starzec
Chalmers University of Technology, 412 96 Göteborg, Sweden

J. Andersson
JA Streamflow, Stockholm, Sweden

Introduction

Stability problems in underground facilities sited in fractured rocks are categorized in regard to the type of geological/physical phenomena causing unfavourable conditions and to the mechanical/structural properties of the excavated medium. One of the major threats to the proper functioning of an underground space is related to the sliding of rigid rock blocks formed by intersecting rock discontinuities.

Studies undertaken by Warburton (1981) and Goodman and Shi (1985) are among the most important contributions in the identification of unstable rock blocks with given orientations of fractures with respect to the dimensions, shape and orientation of an underground facility. One severe limitation of the Block Theory proposed by Goodman and Shi (1985) is the assumption of infinite length of discontinuities intersecting the excavation plane. Whilst this assumption makes the block stability analysis straightforward, in fact it results in a rather unrealistic conceptual fracture network. In effect, both under- and overestimation of the amount and size of unstable blocks

is possible. A remedy to this "imperfection" may be integration of a stochastic discrete fracture network (DFN) with finite fracture sizes.

The rationale of adopting a stochastic DFN approach is that statistics from one- and two-dimensional fracture data can be used for estimating the three-dimensional properties of the fracture network in a rock volume. The fracture statistics in the simulated network follow the observed statistics, but the locations of individual fractures are random. The DFN concept has been implemented among others as a descriptive tool for fracture characterization (Baecher et al. 1977), in fluid flow modelling (Dershowitz 1984; Andersson and Dverstorp 1987; Chilés and de Marsily 1993) and in modelling the performance of geothermal reservoirs (Castaing et al. 1998). Several authors (Hoerger and Young 1990; Shapiro and Delport 1991; Priest 1993; Jakubowski and Tajdus 1995; Dershowitz and Carvalho 1996) advocate the application of DFN for stability assessment of underground spaces, but there are relatively few reported studies on predictions of the occurrence and size of key blocks based on a stochastic three-dimensional fracture network. Verification of such predictions with field observations has attracted growing attention over the past few years, especially for risk assessment for the underground storage of nuclear waste.

As a reliable prediction of unstable rock blocks is directly dependent on the quality of the DFN model, a careful estimation of fracture data and their statistics becomes critical. Fracture network geometry manifests a natural variation and both spatial non-stationarity and trends in data are often observed. This may be a result of tectonic or lithological inhomogeneity at a site. Whether or not there is geological evidence of spatial variability of fracture/joint properties, studies on data homogeneity should always be undertaken prior to evaluation of input parameters for a stochastic fracture network.

This paper presents a statistical evaluation of fracture network properties from a limited amount of data for an area close to Oskarshamn in south-east Sweden with a crystalline rock basement. In addition, an application of the DFN concept for the prediction of key block occurrence in an underground facility for interim storage of spent nuclear fuel CLAB-2, presently being excavated by the Swedish Nuclear Fuel and Waste Management Co., is presented.

The main purpose of the study reported here was to explore means of estimating fracture statistics based on fracture data from only a few boreholes, to derive a stochastic replica of the fracture field at the site and to use the fracture model for estimating the number and size of potential key blocks in an underground cavern. The study involved the following steps:

1. evaluation of the spatial homogeneity of fracture occurrence and intensity by different statistical tests,
2. building a stochastic fracture network model,
3. deriving a probabilistic prediction of the amount and size of potentially unstable rock blocks for the CLAB-2 facility.

Fundamentals of DFN generation

Basic concept of DFN

DFN models belong to the so-called discontinuum model family, i.e. models that represent a body of rock as an assembly of rock blocks separated by discontinuities. As discontinuities occur at a variety of scales, discontinuum models must account for these complexities. The basic principle of stochastic discrete fracture models is that spatial statistics associated with a fracture network can be measured and used to generate fracture networks with the same spatial properties. Application of the DFN concept requires the measurement of fracture geometry in order to construct models that reproduce the observed statistics of the fracture network. This involves specifying a stochastic procedure for generating fractures centred in space, together with their orientations, sizes and other properties.

Many fracture/joint system models have been developed and are continually being improved. Dershowitz and Einstein (1988) summarized the development of the joint system models reported in the literature up to the late 1980s. In spite of the latest progress in the development of the discrete fracture models, the main principles regarding the model input parameters and stochastic generation process remain similar to the early models of Veneziano and Baecher followed by the Dershowitz model (1984); for a description see Dershowitz and Einstein (1988). The fracture network properties of particular engineering significance considered in a discrete fracture network are: fracture size, shape, planarity, relative locations of fractures, spacing between fractures, intensity, orientation, aperture, nature and thickness of the fracture fill material and the genesis of the fractures.

DFN generation procedure

In a stochastic fracture network most characteristic variables are represented as probability distribution functions. The choice of input variables necessary for generating a DFN model depends on both the complexity of the geological conceptual model of the area investigated and the primary purpose and expected results of the modelling. In general, both the fracture network properties discussed in the previous section and the lithology and tectonic history of the area will put constraints on the stochastic fracture field generation.

Based on the field data (fracture mapping on rock exposures and/or borehole logging), fracture network properties are approximated by the best-fit theoretical statistical distributions. Each generated fracture is a product of one Monte Carlo sampling from a number of statistical distributions, each representing a certain fracture property. The combination of all fractures generated in such a manner results in a three-dimensional discrete fracture field. Figure 1 presents one possible three-dimensional fracture network model where fractures are approximated with five- and six-sided polygons with their centres randomly located in space.

In this study, the FracMan stochastic fracture simulator was used for generating the DFN models (Dershowitz et al.

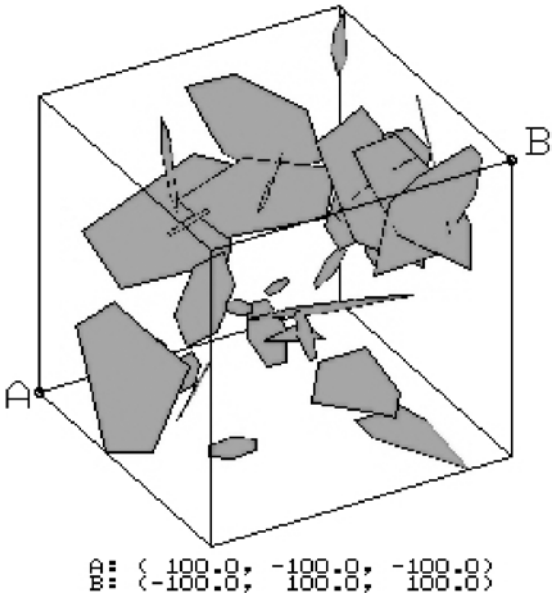

Fig. 1.
Example of a three-dimensional stochastic fracture network generated within the 200 m cube. Fractures are assumed to be five- and six-sided polygons and are randomly located in space

1998). The FracMan code enables generation of a wide spectrum of different conceptual fracture networks, e.g. fracture locations can be random in space or spatially correlated according to fractal scaling, covariance function or other processes. Fracture sizes and orientations can be represented by a number of theoretical probability distributions and fracture shape can be approximated by a variety of geometrical features such as discs, polygons or undulating planes. Finally, the code makes it possible to verify the fracture network model by synthetic line or surface fracture sampling and comparing it with the observed field data.

Statistical stationarity of fracture network properties

Geological homogeneity

The complexity of a DFN model is directly related to the spatial variation of its components, i.e. the variation of the fracture properties. When a modelled area is structurally and/or lithologically heterogeneous, either non-stationary or so-called multidomain DFN models may represent the rock volume in question. Such models demand more extensive field data cover as well as a substantial computer power for the stochastic generation process. If the evidence can be found that the investigated area is geologically/structurally homogenous, a single domain, stationary DFN model can be generated; i.e. a model in which the statistical moments describing fracture network properties (variables) are spatially independent. It appears logical to assume that a geologically homogenous domain will have stationary fracture network variables. However, due mainly to sampling limitations, it is difficult to find sufficient evidence to fully confirm this statement.

Several authors have studied statistical stationarity prior to deriving a conceptual model of a fracture network (Follin and Hermanson 1996; Dershowitz and Ushida 1999). In general, fracture intensity and fracture spacing were taken as the test variables, but stationarity of directional data was also investigated (Geier et al. 1992).

The choice of the procedure for a stationarity test depends on the type and amount of data analysed and on what the results might indicate in terms of geology and fracture occurrence within a studied rock volume. In a classic case there will be a number of boreholes with fracture data or a number of surface mappings within an area and the statistical moments computed at different locations are compared to see if they exhibit spatial variation or not. In cases where the data are sparse, a null hypothesis test may be used instead, i.e. a hypothesis of no difference among sample population mean or median values or the distribution shape for the data sampled at different locations is tested.

As neither the probability distribution the fracture network properties (variables in statistical meaning) actually follow nor the distribution's parameters are known, the most suitable tests for analysing homogeneity/stationarity are non-parametric tests, such as the Kolmogorov-Smirnov (K-S) and Chi-2 tests (Davis 1986; Swan and Sandilands 1995). Comparing K-S and Chi-2, the former can be used for testing both empirical data sets with each other and empirical sets with hypothetical distributions, while Chi-2 is better suited to testing empirical sets against theoretical distributions. Another useful test may be the Mann-Whitney (M-W) test, which is a median value equivalency test (a non-parametric equivalent to the ANOVA test for testing two empirical data sets). The Kruskal-Wallis (K-W) test makes use of the same procedure as the Mann-Whitney test but can be used for testing more than two data sets together (Davis 1986).

Null hypothesis test on fracture intensities at the CLAB site

The CLAB site includes two main underground storage caverns and a system of smaller transport tunnels. The CLAB-1 storage facility is located in south-eastern Sweden and serves as an interim storage for spent nuclear fuel. A new underground cavern known as CLAB-2 is being excavated close to the existing facility, in order to increase the storage capacity. Lithologically, the CLAB area consists of intrusive rocks of granitic composition intersected by aplite and pegmatite dykes (Eriksson 1982). Figure 2 presents a simplified view over the site and the location of both caverns. The positions of the observation boreholes with their azimuths and inclinations are also shown, as well as the locations of the zones of weakness.

One minor and three major weakness zones were identified from surface mapping, refraction seismics and control drilling (Stanfors et al. 1995). In Fig. 2 the major zones are labelled as SZ1, SZ3 and SZ6 and the minor one as SZ7. These zones form an isolated rock block embracing both CLAB-1 and CLAB-2.

It could be suggested that the rock volume bounded by the weakness zones is structurally homogenous in terms of the occurrence of discontinuities. In such a case, only rather weak spatial variations in fracture spacing or intensity would be anticipated within the area. This judgment, however, is based on the assumption that the rock volume delimited by the zones displayed in Fig. 2 is not intersected by any other weakness zones beyond those identified and that the rock mass within the block volume is lithologically homogenous.

In order to support or reject the statement on the homogenous distribution of small-scale discontinuities, non-parametric statistical procedures were applied and the following null hypothesis (H_0) formulated and tested:

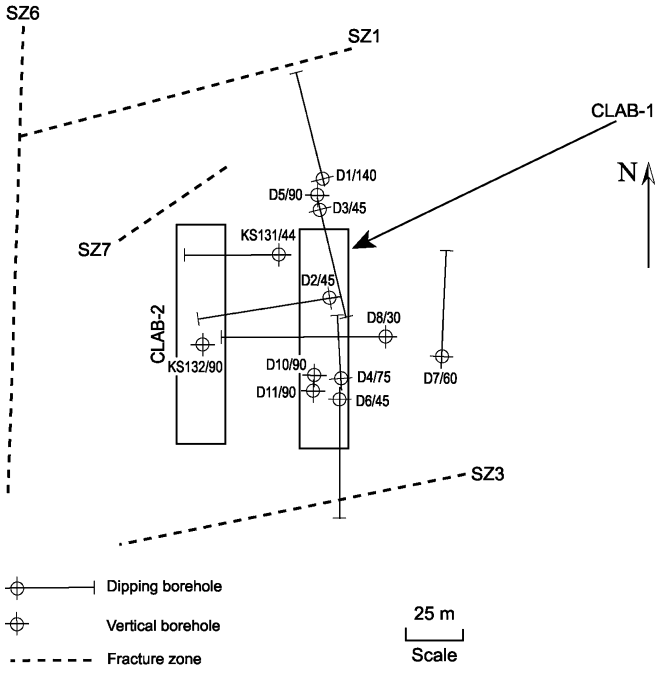

Fig. 2.
Simplified view over the CLAB site

fracture occurrence, expressed either by fracture spacings or intensities sampled at different locations within the rock volume delineated by the weakness zones SZ1, SZ3, SZ6 and SZ7 do not manifest significant differences. On the basis of the outcome from the H_0 test, some inferences about the statistical stationarity of fracture occurrence and in turn about geological/structural homogeneity can be made.

Fracture data for testing the null hypothesis were obtained from the fracture mapping summarized in Table 1. All fractures belonging to the identified cross or weakness zones were discarded from the analysis as these zones had a known orientation and width and hence could be considered as deterministic structures and not as the basic components of the stochastic fracture field it was intended to generate.

With regard to fracture occurrence, only two boreholes (KSI31 and KSI32) provided a complete data record, i.e. the absolute fracture positions along the borehole, orientations, aperture, genetic type and mineral infill. For the other boreholes in Table 1 the spacing data were missing; only fracture intensities measured for each 1 m depth interval were available. For that reason it was not possible to use fracture spacings in the boreholes as the input variables for the null hypothesis test and hence fracture intensities were selected for the H_0 test.

The H_0 test was performed separately for the vertical and inclined boreholes. Additionally, the inclined boreholes were divided into three sub-groups having similar azimuths. All the vertical boreholes (D5, D10, D11 and KSI32) together with KSI31, which deviated from the vertical but had fracture strike and dip data, were corrected for orientation sampling bias following the Terzhagi procedure (Terzhagi 1965) which compensates for fractures subparallel to the sampling line. As the probability of detecting such fractures in the borehole (assuming the borehole is the sampling line) is low compared with the probability of detecting fractures intersecting the borehole at high angles, the data were corrected by increasing the number of fractures that were nearly parallel to the sam-

Table 1.
Summary of fracture mapping from direct core observations and borehole camera for the CLAB site. Fractures belonging to the identified weakness zones are not considered. (Source data: Moberg 1995a, 1995b; Gustafsson and Stråhle 1997)

Borehole (ID/azimuth/inclination)	Length (m)	Average fracture intensity (m^{-1})	Type of data and measurement method
D1/N20°W/40	81	7.59	Fracture intensity (direct core mapping)
D2/N110°W/45	72	6.46	
D3/N160°E/45	82	8.28	
D4/N0/75	67	6.94	
D6/N180°E/45	86	6.58	
D7/N0/60	72	7.43	
D8/N90°W/30	73	5.38	
D10/90	50	7.62[a]	Fracture intensity, fracture dip (direct core mapping)
D11/90	52	7.45[a]	
D5/90	58	7.62[a]	
KSI31/N102°W/44	78	4.46[a]	Fracture positions along borehole, strike, dip, aperture and mineral infill, genetic type (borehole camera)
KSI32/90	61	4.0[a]	

[a]Corrected for orientation sampling bias

pling line. The new, corrected data resulted from multiplying each fracture detected in the borehole by the correction factor w:

$$w = \frac{1}{\cos \alpha} \quad (1)$$

where α is the acute angle between sampling line (borehole) and normal to the fracture plane.

As the inverse of the cosine function for angles close to 90° approaches infinity (i.e. where a fracture is almost parallel to the sampling line), the correction factor w must be assigned an upper limit. Priest (1993) addressed this problem and pointed out that when setting up the limit for the correction factor it is preferable to compare fracture data sampled with differently oriented sampling lines, if possible, mutually orthogonal. He also presented a practical example for correcting for orientation sampling bias with the maximum correction factor close to 10. Genter et al. (1995) applied a maximum factor of 5 for correcting fracture data mapped in nearly vertical boreholes in a granitic massif at Rhein Graben, Alsace, France. Dershowitz et al. (1998) suggest a maximum factor of 7, while La Pointe et al. (1995) used a factor of 5 to correct fracture sampling from the Äspö site (north of CLAB).

In the work reported here a correction factor of 6 was used, which implied that all fractures that had an orientation of more than 77° relative to the sampling line were multiplied by 6 and the rest of the fractures were multiplied by the integer from the ratio $1/\cos\alpha$. At this stage, the advantage of correcting for orientation sampling bias was that fractures belonging to differently oriented boreholes could be considered for the null hypothesis testing.

The H_0 test on fracture intensities using the Kruskal-Wallis (K-W) procedure was undertaken on more than two data sets/boreholes, while the Mann-Whitney (M-W) test was carried out on two data sets. Table 2 presents the results from the K-W and M-W tests for all twelve boreholes shown in Table 1. The K-W test on the sample populations in boreholes D1, D4 and D7 and D5, D10 and D11 showed that within each tested group the median fracture intensities were not significantly different. Similar results were obtained from the M-W test for KSI31 and KSI32. The results of both tests were obtained for 5% level of significance. Summarizing the results outlined in Table 2, it was found that there was no statistical evidence on which to reject the hypothesis that:

1. fracture intensities along north-dipping boreholes belong to a statistical population with the same median value,
2. fracture intensities along vertical boreholes belong to a statistical population with the same median value,
3. fracture intensities measured with a borehole camera belong to a statistical population with the same median value.

For the boreholes dipping to the west and south, however, the null hypothesis was rejected.

It should be noted that fracture data from all boreholes suffixed "D" (Fig. 2) were collected from direct core observations, while data from KSI31 and KSI32 were obtained from a borehole camera. In practice, this may mean that some fractures identified from core observations may not be found using a borehole camera and vice versa, and it is important to appreciate that interpretation of the results from statistical tests on data obtained by applying different measurement methods might be ambiguous.

In order to complement the median value test, another null hypothesis test based on Kolmogorov-Smirnov (K-S) statistics was undertaken. When using K-S statistics the overall shape of the cumulative frequency plots of sample data sets can be compared. In this study the K-S test was designed following the procedure outlined in Gibbons and Chakraborti (1992). The K-S test derives the largest difference in cumulative frequency histograms between sample distributions and relates this difference to some tabulated critical values (Davis 1986).

Table 3 presents the results from the K-S test on fracture intensities for pairs of boreholes having similar orientations and for which the same fracture detection methodology was applied. If the K-S statistics depicted as $K\text{-}S_{stat}$ exceed the critical value statistics $K\text{-}S_{crit,}$ the null hypothesis stating that the two tested sample sets belong to the same statistical population is rejected. The K-S test was run for a 10% significance level. Except for two pairs of boreholes (D6-D3 and D2-D8), the $K\text{-}S_{stat}$ was lower than the critical value $K\text{-}S_{crit}$ (see Table 3), hence the null hypothesis could not be rejected. Indeed, even for the

Table 2.
Kruskal-Wallis (*K-W*) and Mann-Whitney (*M-W*) non-parametric null hypothesis (H_0) tests on fracture intensities for groups of boreholes exhibiting similar orientations and the same fracture measurement methods. Null hypothesis assumes that fractures in a specific group belong to the same statistical population

Boreholes tested	Test type	Testing results
D1-D4-D7 (dipping to N)	K-W	H_0 not rejected
D6-D3 (dipping to S)	M-W	H_0 rejected
D2-D8 (dipping to W)	M-W	H_0 rejected
D5-D10-D11 (vertical)[a]	K-W	H_0 not rejected
KSI31-KSI32[a]	M-W	H_0 not rejected

[a]Corrected for orientation sampling bias

Table 3.
Kolmogorov-Smirnov (*K-S*) test of a hypothesis that fracture intensities along tested boreholes belong to the same statistical population. If $K\text{-}S_{stat}$ exceeds the critical value $K\text{-}S_{crit}$, the null hypothesis is rejected at 10% significance level

Boreholes tested	$K\text{-}S_{stat}$	$K\text{-}S_{crit}$
D1-D4	0.16	0.20
D1-D7	0.03	0.20
D4-D7	0.14	0.21
D6-D3	0.23	0.19
D2-D8	0.22	0.20
D5-D10[a]	0.11	0.25
D5-D11[a]	0.07	0.25
KSI31-KSI32[a]	0.12	0.21
KSI31-D5[a]	0.17	0.21

[a]Corrected for orientation sampling bias

fracture intensities sampled with two different measurement methods (e.g. KSI31and D5), the null hypothesis could not be rejected.

Summarizing the H_0 testing, more evidence was found to accept the hypothesis that fracture intensities recorded within the investigated area/volume do not significantly differ than to reject it. The results for the boreholes dipping to the west and south could be explained by an increased sensitivity to orientation sampling bias or by the fact that some of the boreholes were intersected by a minor weakness zone/zones which were not verified with refraction seismics, surface mapping or control drilling. Such zones could substantially increase fracture intensities in some boreholes and significantly influence the test results. In general, it is considered that where fracture intensities were corrected for orientation sampling bias, the results were more reliable and that the investigated area is homogenous as regards fracture intensity. Nevertheless, further tests were carried out to investigate whether fracture intensity follows any vertical trend, using the moving average of fracture intensities for 1, 3 and 5 m windows along the boreholes, correlated for sampling bias. The results showed no evidence that fracture intensities are depth-dependent.

From both geological judgment and statistical tests of homogeneity/stationarity, therefore, it was concluded that fracture occurrence at the CLAB site is spatially independent but that the hypothesis that the discontinuities within the considered rock volume belong to the same structural unit had not been disproved.

Input variables for discrete fracture model at the CLAB site

It was further postulated that the fracture parameters evaluated from KSI31 and KSI32 would be representative for the whole modelled rock volume. The prime reason for selecting these two boreholes as the major source data for the stochastic fracture field generation was the fact that they provide the most complete data record (fracture orientations, spacing, aperture and genetic type), while the data from the other boreholes were limited to only fracture intensity.

Type of discontinuities

The selection of the appropriate discontinuities to form the basis for a stochastic fracture network was contingent at first on their ability to act as sliding planes for potentially unstable rock blocks. Not all discontinuities detected in the boreholes KSI31 and KSI32 were equally important for block stability calculations, due to their genetic character, size and/or fracture roughness.

According to Gustafsson and Ståhle (1997), who analysed fracture data from borehole camera images in boreholes KSI31 and KSI32, it was possible to distinguish three main types of discontinuities: fractures filled with minerals, open fractures and veins filled with pegmatite or fine granite. Some mineral-filled fractures contained small cavities, but it was difficult to assess if the presence of the cavities would eventually contribute to either reduction or increase in friction along fracture planes. With only six open fractures in the 592 discontinuities detected in the two boreholes, the amount of open fractures found was too low to consider them as a statistically relevant group for stochastic network modelling.

An appropriate selection of the type of discontinuities for model generation was important not only from the rock engineering point of view but also because the generation of a DFN model representing all the types of discontinuities detected with a corresponding fracture intensity of about 4 m^{-1} (see KSI31 and KSI32 in Table 1) would make considerable demands on computer power and time.

Field observations from several underground projects in Sweden carried out in similar geological environments to the CLAB site have shown that some discontinuities can be more sensitive than others in terms of block sliding (U. Lindblom, personal communication, 2000). As any selection of discontinuities based on their mechanical properties (e.g. friction or shear strength) was difficult on the information available from the boreholes, a discontinuity size criterion was adopted and referred to the empirical relationship between joint size and aperture observed by Vermilye and Scholz (1995) on granodiorite outcrops at Florence Lake, USA. In other words, the discontinuity aperture data valid for the CLAB site obtained from borehole camera measurements in KSI31 and KSI32 together with the mentioned joint length to aperture ratio were used as the basis for classifying the discontinuities in accordance with the inferred joint/discontinuity length. For this study it was decided that all discontinuities with an aperture equal to and larger than 5 mm would constitute the statistical grounds for the DFN model generation. It should be pointed out that according to Gustafsson and Ståhle (1997), the aperture is defined as the thickness of the altered zone and not as the width of the opening available for fluid flow, except for the open fractures where the hydraulic definition of the aperture was applied.

The majority of the discontinuities selected for the further stochastic generation procedure were veins filled with fine-grained granite or pegmatite, some of which were tectonized. The rest were fractures filled with chlorite or calcite. In addition, all the open fractures found in the boreholes, irrespective of their aperture size, were assigned to this group due to the anticipated relatively low shear strength on their planes and higher potential to trigger block sliding.

Although the adopted size criterion and especially the cut-off range for apertures was to some degree arbitrary, it was considered that larger discontinuities were more important for block stability analysis than small ones. In summary, 87 veins and fractures from boreholes KSI31 and KSI32 were chosen. Henceforth for brevity the term fractures will be used as the collective name for the selected discontinuities.

Fracture orientation

When the number of observed fractures with a known orientation is large and the fractures exhibit signs of clustering on a stereoplot, the separation of the fractures into distinct orientation sets can improve the reliability of a DFN model. In practice, the separation into orientation sets and clustering of fractures relies both on studies of the tectonic history of a site, rock stress distribution and the mechanical properties of rocks and on statistical separation algorithms. Interested readers are referred to Priest (1993) who presents basic principles and some practical examples for identification and delimiting orientation fracture sets. In addition, the work of Mardia (1981) and Herda et al. (1991) present some interesting aspects of the analysis of directional data. A purely statistical separation into orientation sets minimises subjective bias when attempting to infer orientation of clusters from a study of the tectonic history of the area, yet the outcome from such an analysis should always be complemented with the existing geological information.

Figure 3 presents the lower hemisphere projection of poles to fractures that were selected for the stochastic DFN model generation, i.e. the fractures from boreholes KSI31 and KSI32 that fulfilled the size criterion referred to above. The data were corrected for orientation sampling bias using a correction factor of 6. This correction resulted in the increase of the originally observed number of fractures from 87 to 112.

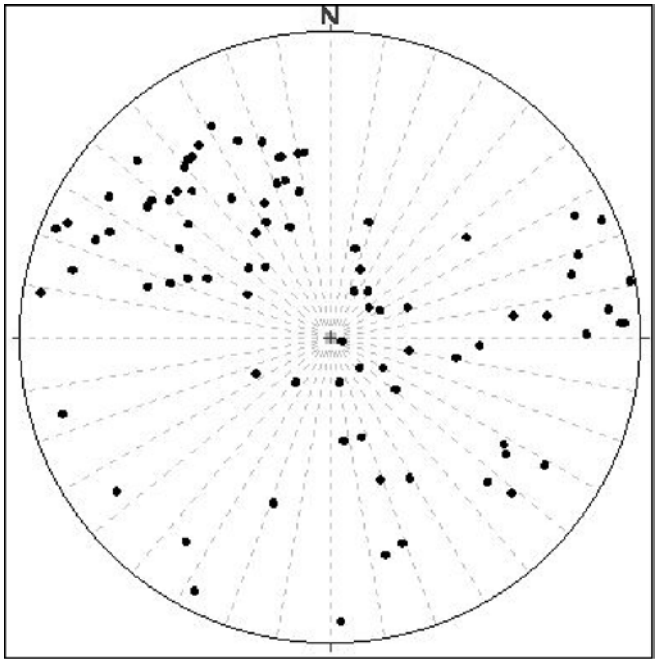

Fig. 3.
Poles to fractures (veins and discontinuities with apertures equal to and larger than 5 mm) detected by borehole camera in boreholes KSI31 and KSI32. Lower hemisphere projection. Fractures correlated for orientation sampling bias with a correction factor of 6. Number of fractures after correction: 112. (Source data in Gustafsson and Stråhle 1997)

In order to separate fractures into orientation sets, the Interactive Set Identification System (ISIS) of Dershowitz et al. (1998) was used. In short, the essence of ISIS is that the statistical properties of each set are first derived from the statistical properties of the fractures assigned to the set, then those fractures that have a low probability of being part of that set are removed and reassigned. The set separation procedure begins with visual identification of all possible sets, then each set is approximated with a number of hypothetical statistical distributions until the best-fit probability function is found.

Four different orientation sets were at first determined visually from Fig. 3. For each set a number of hypothetical distributions were tested to find the best-fit probability distribution function (pdf). The best match was found with Fisher's pdf (Davis 1986), which is an equivalent to normal distribution for oriented data on a sphere. Table 4 summarizes the set separation analysis performed with the ISIS algorithm and provides K-S "goodness-of-fit" statistics between the observed and corrected orientation data classified into each set and the theoretical statistical distributions.

Each orientation set in Table 4 was characterized by its mean pole trend (azimuth) and plunge (inclination) vectors, a dispersion coefficient κ, K-S "goodness-of-fit" statistics and the amount of fractures expressed as a percentage of the previously selected and corrected total, i.e. 112 fractures. The dispersion coefficient is a measure of a sample population scatter about the mean pole vector representative for the whole set. Higher values of κ imply less scatter. Regarding K-S statistics, following the procedures adopted in FracMan, a significance higher than 95% indicates the statistically satisfactory fit of the theoretical pdf with the observed data.

Of the identified orientation sets, only set 2 satisfied the last criterion, i.e. the theoretical Fisher's distribution with κ=17.1 fitted to the observed data with a high enough statistical confidence. The rest of the best-fit pdf's showed too low a statistical significance to be considered reliable probabilistic estimates of the observed data.

When fracture orientation data are scarce, as they were for the CLAB site, and satisfactory fitting between possible orientation clusters and theoretical probability distributions cannot be obtained, "bootstrap" sampling (Efron 1982) might be a better alternative (Hermanson et al. 1999). "Bootstrapping" implies that fractures that are to be generated in a stochastic DFN model have the same

Table 4.
Summary of orientation set identification based on ISIS procedure (Dershowitz et al. 1998) Number of fractures n=112. All sets were best fitted to Fisher's probability distribution

Orientation set: mean pole (trend, plunge)	Dispersion coefficient, κ	K-S statistics, statistical confidence, %	Fracture percentage of the observed total
Set 1 (68, 6)	8.8	0.173, 37.2	24.8
Set 2 (69, 79)	17.1	0.108, 96.6	18.6
Set 3 (162, 27)	7.2	0.183, 54.5	16.8
Set 4 (318, 36)	15.4	0.126, 44.6	39.8

orientations as observed in the field and no set separation is performed. The dispersion coefficient for "bootstrapping" can be estimated by using the formulae for dispersion coefficient for Fisher's distribution (see Priest 1993 for detailed explanation).

Even if previous field investigations in the areas proximal to the CLAB site had indicated that discontinuities follow distinct orientation sets and hence clustered around up to six major orientation vectors (Ericsson 1987), it was difficult to find such a tendency for the fractures in KSI31 and KSI32, relying on the performed ISIS analysis. Additionally, due to the small amount of data, the visual identification of clusters from the stereoplot in Fig. 3 might be severely biased due to the subjectivity of individual interpretation. In view of these concerns, the orientation input data for the stochastic DFN model generation were derived as "bootstrap" sampling directly from the orientations of the 112 selected fractures, applying a dispersion coefficient of 50.

Spatial model

Inasmuch as technical and economic limitations did not allow a complete investigation of the relative positions of fractures everywhere within the modelled rock, finding a representative pattern of spatial distribution for fracture locations was not an easy task. Spatial distribution of fractures is usually inferred from fracture positions/spacing measurements along sampling lines or from two-dimensional rock exposure mapping. However, the orientations of discontinuities and their sizes also have a bearing on the spatial pattern.

Priest (1993) presents a more in-depth study of these topics and, in the absence of clear evidence for fracture clustering, proposes the adoption of random fracture location models based on a Poisson process. Random locations of fractures were discussed in the early work of Priest and Hudson (1976), Baecher et al. (1977) and Wallis and King (1980) who observed that fracture spacing tends to follow exponential distributions, suggesting the random location of fracture centres in space.

Although the assumption of random fracture locations considerably simplifies fracture network generation procedures, there is still some incentive to investigate spatial relationships among fractures before setting up a DFN model. For example, Geier and Thomas (1996) found that the Levy–Lee and Nearest-Neighbour fracture locations models provided a better fit with observed data than a random locations model for the Äspö area located close to the CLAB site. Chilés (1988) reported that fractures mapped in the Fanay-Augéres (France) uranium mine were not purely randomly located. Barton and La Pointe (1995) summarized the work of several authors on fractal patterns in geology and presented examples for fractal scaling of fracture spacing. This would suggest that there is field evidence that fractures may be spatially organized according to some other processes and may not be purely random.

In the authors' opinion the analysis of spatial patterns makes more sense if fractures are separated into orientation sets (assuming such sets exist), rather than analyzing all mapped fractures together. Priest (1993) pointed out that in some cases fractures are spatially organized within orientation sets but demonstrate random location patterns when all the sets are grouped together. It is considered that the opposite would also be possible, hence the analysis of fracture location patterns for the CLAB data was first undertaken separately on each orientation set identified within each borehole by the ISIS procedure (even if they were not found to be statistically significant). Subsequently, the same analysis was carried out on all fractures within each borehole without set separation. The location patterns were analysed by means of power spectrum density and power semivariogram functions.

The analysis of fracture spatial patterns for the CLAB site was performed on fracture spacing data obtained from boreholes KSI31 and KSI32. These were the same data as used previously for the ISIS set separation analysis, i.e. 112 fractures corrected for orientation sampling bias. Input data for spectral density and power semivariogram analysis were computed from fracture intensities within a 1 m window along the boreholes.

The interpretation of power density plots and power semivariograms relies on similar principles, yet subtle differences exist. A power density function was computed by breaking the profile with calculated fracture intensities along the borehole into a sum of sinusoidal components, each with its own wavelength, amplitude and phase. The individual variance of each component is related to the amplitude of the waveform. The power spectrum is calculated as the sum of the squared amplitudes of each sinusoidal component, that is the sum of individual variances of all the sinusoidal components. By plotting the power spectrum versus the inverse of the wavelength it is possible to determine whether fracture intensities are spatially variant and, if so, which components (short or long wavelengths) contribute to the largest variability.

The slope of the spectral density plot can be used to assess different possible spatial models. If the spectrum is fractal (self-similar) it will plot approximately along a straight line. Consequently, the slope of the straight line relates to the fractal dimension. A slope of zero implies that fractures in the borehole are located according to the Poisson process. The steeper the slope, the higher the variance in fracture intensities for long-wavelength components as compared to the variance for short-wavelength components. This would indicate that fractures tend to form tighter clusters. For more details on spectral analysis readers are referred to Båth (1974) who outlined the fundamentals of the spectral methods and their application in signal analysis. An interesting summary on the implementation of power spectrum in characterizing fracture roughness was presented by Brown (1995).

The semivariogram function for fracture intensities relates the sum of the squared differences between fracture intensities at two different locations along the sampling line to the locations' separation distance. When plotting semivariogram versus increasing separation distance,

inferences can be drawn regarding spatial correlation pattern and in some instances, the size of fracture clusters or the distance between clusters may be estimated. There are extensive literature reviews on semivariogram analysis and its application in the earth sciences; for a good introduction to the subject with practical examples, see Isaaks and Srivastava (1989).

When the semivariogram plotted on double logarithmic scale results in an approximately straight line, it is considered to be fractal. The fractal dimension D is given by the formula D=2–a/2, where a is the slope of the semivariogram (P. La Pointe, personal communication, 1999). Values of D can range from 1.0 to 2.0. The fractal dimension D=1.5 implies no spatial correlation, i.e. Poisson process.

From the analysis with orientation set separation, only set 4 in borehole KSI32 showed some indication of weak fracture clustering (Table 4). Figure 4 depicts the spectral density and Fig. 5 the power semivariogram, i.e. the semivariogram with double logarithmic scales for the fracture intensities belonging to this set. The power spectrum in Fig. 4 was fitted with a straight line with the regression coefficient R=0.7. The fractal dimension estimated from the slope of the regression line was D=2.05 [see Turcotte and Huang (1995) for the computation formula]. The fractal dimension estimated from the semivariogram slope in Fig. 5 was D=1.98.

The spatial pattern analysis without set separation showed that fractures in borehole KSI32 exhibited some "delicate" indications of clustering, while the power spectrum and power semivariogram for KSI31 were nearly flat, i.e. the fractures were most probably randomly located in the borehole. The fractal dimension estimated from the spectral density plot for KSI32 was found to be D=1.96 (R=0.87). The fractal dimension found from the power semivariogram was nearly the same: D=1.98.

The fracture location pattern for set 4 and for the whole of borehole KSI32 showed very similar trends. It is considered likely that the spatial pattern of set 4 dominated the spatial pattern in the whole of KSI32 as this set was found to constitute the majority of the fracture population in the boreholes (see Table 4). The fact that the fractal dimensions identified from both the spectral and semivariogram analyses oscillated around 2.0 implies that the fracture system as inferred from the two boreholes was negatively correlated, i.e. fractures may form very weak, non-isolated clusters and tend to form one big network. On the contrary, if the fractal dimension approached 1.0, the system would be positively correlated with very pronounced isolated fracture clusters.

The results from the fracture location patterns analysis did not provide enough confidence to state that the fractures would form any apparent isolated clusters. Thus, in the absence of clear evidence of spatial correlation, it was assumed that the fracture location pattern at the CLAB site was random.

Fracture size

It is nearly impossible to determine the correct fracture size without dismantling a rock volume of interest and measuring the size directly. Alternatively, by approximating fractures using geometrically regular objects/surfaces such as disks or polygons and with access to trace length data from planar exposures, reasonable estimates of fracture size can be made (Baecher et al. 1977; Warburton 1980; Priest 1993).

It is noteworthy that veins constituted the vast majority of the discontinuities selected for stochastic DFN generation at the CLAB site. However, no vein trace length data were available, hence the fracture size was estimated using the empirical relationship between joint length and aperture.

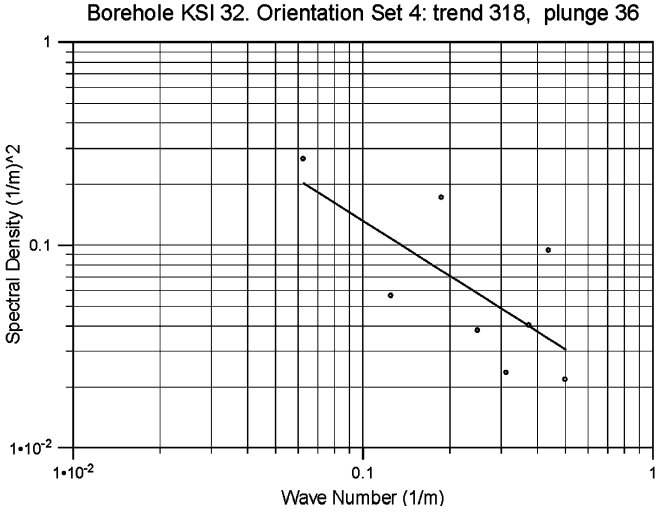

Fig. 4.
Spectral density plot of fracture intensities for orientation set 4 in borehole KSI32. Units on vertical axis express the squared amplitude of fracture intensity in $(m^{-1})^2$ at 1 m intervals along the borehole; units on horizontal axis are in m^{-1}. Wave number $k=2\pi/\lambda$, where λ is wavelength (in m). Spectral density plot was fitted with regression line with the slope α=0.91 and regression coefficient R=0.7

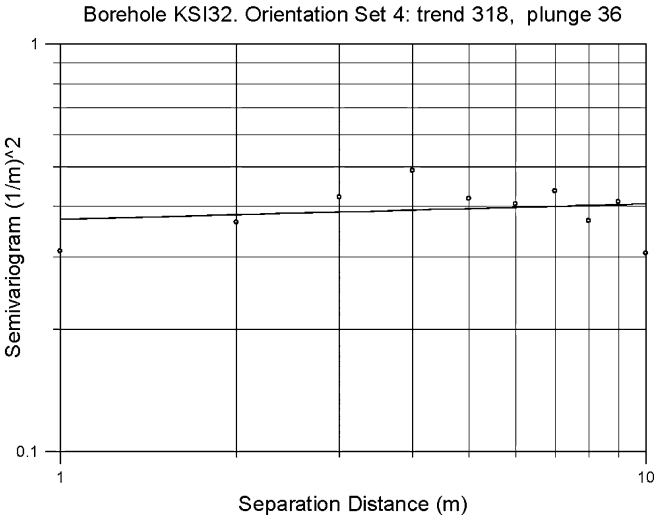

Fig. 5.
Power semivariogram for fracture intensities for orientation set 4 in borehole KSI32. Units on vertical axis are the squared fracture intensity in $(m^{-1})^2$ at 1 m intervals along the borehole; units on horizontal axis express the separation distance in m. Slope of the fitted straight line a=0.04

In this study, fracture size estimation was based on the work of Vermilye and Scholz (1995) who derived an empirical relationship between aperture and joint length for veins mapped on granodiorite outcrops at Florence Lake district, USA. They found the average aspect ratio between aperture and length to be 1.9×10^{-3}.
It should be stressed that the decision to adopt this aspect ratio in the present study was based on the lithological similarities between the CLAB and Florence Lake sites; other aspects of vein formation such as the tectonic history of both sites were not considered. For this reason, the estimated fracture sizes for the CLAB data should be considered as very approximate. Nevertheless, as the fracture apertures were known from the borehole camera studies in KSI31 and KSI32, it was considered reasonable to estimate fracture size using measured apertures rather than base it on any generic assumptions from general knowledge of the Swedish crystalline bedrock.
Initially, for each of the 112 fractures from KSI31 and KSI32 the representative fracture radius was calculated from the known aperture and the adopted aspect ratio of 1.9×10^{-3}. It was assumed that the fractures had the shape of circular discs. In the next step, the obtained fracture radii were fitted with a number of theoretical probability density functions. The best fit was found for log-normal distribution with a mean of 11.9 m and standard deviation of 26.5 m. Figure 6 presents the best-fit pdf and the estimated fracture radii data.

Volumetric fracture intensity and termination type

There are two ways in which fracture intensity can be generated in the FracMan code: (1) by specifying the total number of fractures within a generation region, and (2) by specifying a volumetric intensity measure termed the P_{32} parameter. P_{32} is the ratio between the total area of all fractures and the total volume of the material in which the fractures are generated. Although P_{32} cannot be measured in situ, this parameter is linearly correlated to fracture intensity, which can be measured along a borehole or on a rock exposure. The proportionality constant depends on the fracture orientation and distribution of the fracture size (Dershowitz and Herda 1992).
In the current study, P_{32} was used to build the stochastic DFN model for the CLAB site. Using P_{32} as the fracture intensity measure rather than the total number of fractures generated in the model makes the verification of the model with the field data more straightforward. As mentioned above, P_{32} is related to the observed fracture intensity. As fracture intensity from outcrop mapping at the CLAB site was not available, the estimation of P_{32} was based on the observed fracture intensity in boreholes KSI31 and KSI32. For convenience and following the FracMan nomenclature, in the remainder of this paper the one-dimensional fracture intensity will be expressed using the parameter P_{10}. The observed P_{10} for KSI31 and KSI32 for the previously selected fractures was found to be 0.62 and 0.64 fractures m^{-1} respectively. The procedure for assessing the correct P^{32}, i.e. the one reflecting the real fracture intensity in the modelled rock volume, is given under the heading "Stochastic fracture network generation for the CLAB site" as this procedure is, in fact, a part of the model-generating process itself.
Another important component to be considered in discrete fracture modelling is the connectivity of the fracture network. This is a crucial aspect in DFN models for flow simulation but also of great importance in rock mechanics where rock volume is treated as an assembly of rock blocks isolated by the discontinuities and the perimeter of an underground opening. When fractures cease in a rock matrix without intersecting other fractures, the rock is potentially less blocky and bridges between discontinuities will contribute to a higher stability of the excavation. In contrast, when fractures constitute densely interconnected complexes, there is a higher tendency for development of rock blocks, which, depending on the fracture orientations and size, may jeopardize the safety of the underground space. The tendency of blocks to slide under gravity forces, as well as their shape and volume, also depends on the way fractures terminate, i.e. whether the fractures terminate at one end or are entirely bounded by neighbouring discontinuities. Depending on the spatial model chosen, the FracMan code allows either a total percentage of terminations or a termination probability to be specified.
For the purpose of this study the only available fracture termination data in areas close to the CLAB site comprised a total of 63,000 mapped discontinuities from the Äspö area located several kilometres north of the CLAB site (S. Tirén, personal communication, 2000). According to Tirén, about 20% of the mapped discontinuities terminate against other fractures at one end and in the rock mass at the other. However, these findings had still not been fully verified when this paper was completed. In addition, Tirén's study involved interpretation of all types of discontinuities and did not take into account fracture genesis, hence the 20% termination should be considered as a tentative assessment and not as a definitive result.

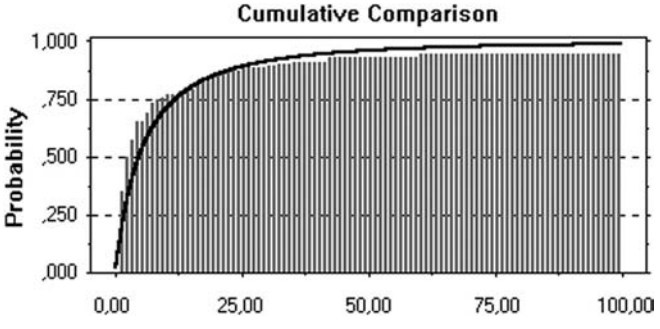

Fig. 6.
Cumulative log-normal probability best-fit plot (thick line) to fracture radii in m (vertical bars) estimated from the aperture data for fractures selected from boreholes KSI31 and KSI32

Stochastic fracture network generation for the CLAB site

The aim of the initial fracture network generation was to determine the real fracture intensity (expressed with P_{32})

and in turn correlate the stochastic fracture field with the observed fracture data. To reflect the observed fracture spatial location pattern, the "BART" conceptual model was adopted (Dershowitz et al. 1998). In the BART model, fracture centres are located uniformly in space, following the Poisson process. However, fracture termination modes which result in non-uniform fracture locations are allowed. Fracture termination was assigned by the termination percentage $T_{\%}$. At first 1–$T_{\%}$ fractures were generated based upon uniformly located fracture centres. $T_{\%}$ fractures terminating at intersections were then generated from locations uniformly positioned on the surface of existing fractures. These positions were not the fracture centres, but rather the locations at which the fracture termination occurred. The fractures generated from these locations were defined with centres at a distance away from the termination locations such that the fracture surface area distribution for the generated fractures was preserved.

The generated fracture shapes were approximated with eight-sided polygons. The representative fracture radii were generated from a log-normal probability distribution with a mean of $\overline{R} = 11.9$ m and a standard deviation σ_R=26.5 m (see Fig. 6). The orientations of fractures were "bootstrapped" directly from the 112 fractures selected from boreholes KSI31 and KSI32 and correlated for orientation bias. The fracture termination percentage $T_{\%}$ was set at 20%. The generation region for the fracture field was a cube with dimensions 180×180×180 m. The model size exceeded the volume actually needed for further tunnel stability simulations but was kept oversized to minimize edge effects.

As the first step, three DFN models with different initial P_{32} were generated. Each DFN generation process included 10 Monte Carlo realizations. Accordingly, eight synthetic boreholes were positioned within the generation region; half of the boreholes had exactly the same length, radius and orientation as the KSI31 borehole but were located at different places inside the model and the other half of the boreholes reflected the characteristics of KSI32. After generating each of the three DFN models, synthetic sampling with eight boreholes was carried out and the linear fracture intensity (P_{10}) for each borehole was calculated. This procedure identifies the best initial P_{32} to guarantee a similar number of fracture intersections in the synthetic sampling and the observed samples. The model for which the P_{10} was found to be closest to the observed fracture intensity was used for the estimation of the "true" value of P_{32}. Using the relationship between P_{32} and P_{10} mentioned earlier, following Dershowitz and Herda (1992):

$$P_{32True} = P_{32Simulated} * P_{10True} / P_{10Simulated} \quad (2)$$

where P_{32True} is the real fracture intensity to be estimated, $P_{32Simulated}$ is the initial (guessed) intensity, P_{10True} is the observed fracture intensity and $P_{10simulated}$ is the fracture intensity obtained from synthetic sampling in the model. Applying Eq. (2) and averaging the $P_{10Simulated}$ from 80 synthetic samplings (ten Monte Carlo realizations multiplied by eight synthetic boreholes), using the initial $P_{32Simulated}$=1.2 m^2/m^3, it was found that P_{32True}=1.05 m^2/m^3. To verify the DFN model, ten additional Monte Carlo realizations were run with P_{32}=1.05 m^2/m^3 as the "true" intensity and keeping all other model parameters the same. From the synthetic sampling averages of P_{10}=0.6 and 0.66 m^{-1} for KSI31 and KSI32 respectively were obtained. It will be appreciated that the observed fracture intensity was P_{10}=0.62 m^{-1} for KSI31 and P_{10}=0.64 m^{-1} for KSI32. Thus, there were almost negligible discrepancies between the simulated and observed fracture intensities – only 0.02 m^{-1}.

It was concluded that the DFN model generated with P_{32}=1.05 m^2/m^3 satisfactorily represented the fracture network at the CLAB site. Table 5 summarizes the input variables for the generation of the final DFN model.

Analysis of block stability for the CLAB facility

This section presents the results from the numerical identification of potentially unstable blocks for the CLAB-2 excavation, which is proposed to serve as an interim storage facility for spent nuclear fuel. The CLAB-2 cavern has the shape of a horseshoe tunnel about 115 m long, 21 m wide and 27 m high. The tunnel is located about 30 m under the ground surface and its long axis strikes N–S (see Fig. 2).

The key blocks statistics were performed by using the RockBlock computer code developed by Golder Assoc., Seattle (Dershowitz et al. 1995). After entering the stochastic DFN model, the RockBlock code performs five consecutive operations:

1. Fracture intersections are computed.
2. Trace maps defined by fracture intersections with the tunnel structure are built.
3. Rock blocks for the entire interior of the tunnel are identified.
4. The volume and mass of rock blocks are determined.
5. Stability analysis is performed.

This study focused exclusively on potentially unstable blocks, i.e. friction along fracture planes and the distribution of rock stress around the tunnel perimeter were

Table 5.
Components of the discrete fracture model for the CLAB site

Type of discontinuities	All veins, open and filled fractures with apertures equal to and larger than 5 mm
Spatial model	BART (Poisson process)
Fracture orientations	Bootstrap, dispersion κ=50
Fracture shapes	Eight-sided equilateral polygons
Fracture size (representative radii)	Log-normal distribution, $\overline{R} = 11.9$ m, standard deviation σ_R=26.5 m
Volumetric fracture intensity	P_{32}=1.05 m^2/m^3
Fracture terminations	$T_{\%}$=20%
Model size	180×180×180 m^3

ignored. The last step in the RockBlock procedure was therefore valid for the conditions at which only gravity forces act on the rock blocks. For block weight calculation the rock mass density ρ=2.6 g/m^3 was applied (Eriksson 1982). For the rock block simulations, a synthetic six-panel horseshoe tunnel with the same dimensions as the real CLAB-2 facility was sited inside the stochastic DFN model generated according to Table 5.

The initial simulations with RockBlock showed that the computation of rock blocks for the 180 m DFN cube was severely restricted by the available computer power and time. As a consequence, the size of the model was reduced to a slab with dimensions of 140 m long, 50 m wide and 50 m high. It was believed that the edge effects would not adversely affect the block analysis as the model dimensions along each co-ordinate exceeded the dimensions of the tunnel by a length larger than the mean of the generated fracture radii.

The block analysis was carried out for 30 Monte Carlo realizations of the stochastic DFN model. For each realization, the number of blocks formed in the tunnel roof and walls was obtained together with their mass and stability status. Figure 7 presents the visual outcome of the block analysis for one Monte Carlo DFN realization for a 10 m section of the tunnel. The key blocks are marked with arrows.

Although the visual effect and the block characteristics derived from the block analysis may look impressive, the interpretation of the results is not easy. It should be kept in mind that the rock block calculations presented here are based on the stochastic fracture model; consequently, the derived block locations along the tunnel cannot be considered as the real block positions; the number of blocks and their size must be related to the actual length of the excavation.

The block analysis was undertaken for two distinct tunnel orientations: N–S and E–W. The first orientation agreed with the real tunnel trends for both the CLAB-1 and CLAB-2 facilities. Predictions for each orientation should be interpreted separately, but comparison of the results from distinct orientations illustrated one way of utilizing such predictions in a decision-making process where more than one option for the location of a tunnel/underground space would be possible.

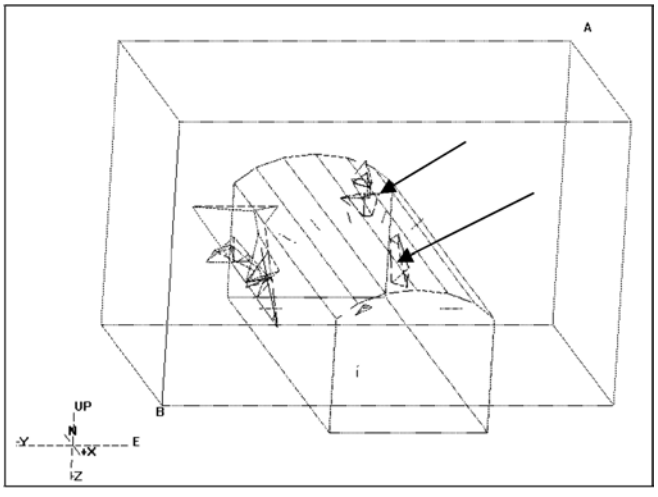

Fig. 7.
Visualization of key block analysis for a randomly chosen 10 m interval in the CLAB-2 facility undertaken using the RockBlock computer code. Arrows point at potential key blocks

Block simulations for N–S tunnel orientation

After combining all Monte Carlo simulations it was found that the majority of blocks had a very small mass. Consequently, all blocks of less than 10 tonnes (t) in weight were arbitrarily discarded from the further analysis as they were considered to be of limited importance as regards the stability of the cavern. Assuming a regular geometric shape, a 10 t block is equivalent to a cube with sides of 1.6 m. The amount of key blocks N in the cavern's walls and roof was best fitted with a log-normal probability density function with the expected mean M_N=123 and the standard deviation δ_N=14 (Fig. 8).

The probability density distribution and the predicted block mass are depicted in Fig. 9. From this plot the proportion of the blocks within a specified weight range can be estimated in respect of the total number of unstable blocks. It is also possible to estimate a probability for finding blocks with a mass above or below a certain critical threshold. The predictions regarding a block mass M were

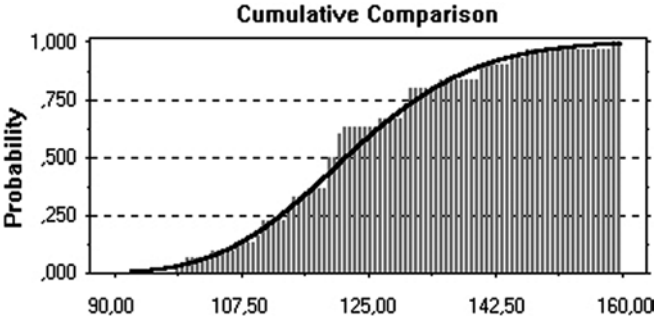

Fig. 8.
Simulated number of key blocks (vertical bars) for the CLAB-2 facility for the N–S tunnel and best-fit log-normal probability plot (thick line). Population mean M_N=123, population standard deviation δ_N=14

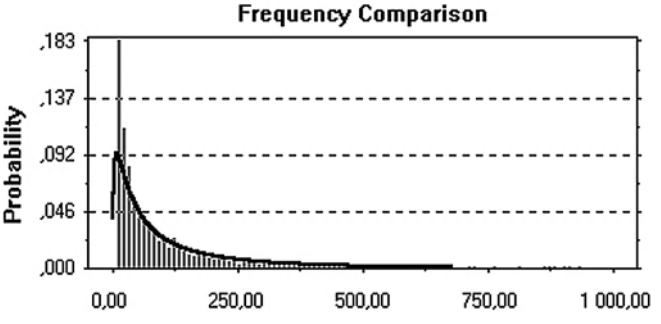

Fig. 9.
Simulated block weights in tonnes (vertical bars) and the best-fit log-normal pdf plot (thick line) for the CLAB-2 N–S tunnel. Population mean M_W=235 t, population standard deviation δ_W=638 t

approximated with a log-normal probability distribution with the expected mean M_W=235 t and the standard deviation δ_M=627 t. Despite excluding all blocks with a mass of less than 10 t, the majority of the identified blocks were still relatively small. For the benefit of clarity of the plot, the horizontal scale in Fig. 9 was shrunk to about 1,000 t as the amount of blocks beyond this range was very low, making plotting and interpretation of such data difficult. The largest block predicted from all 30 Monte Carlo simulations had the mass of 63,000 t; however, the probability of finding such a block was extremely low.

Block stability for the E–W tunnel

The same type of predictions presented for the N–S tunnel were also made for the E–W direction. To make the results comparable between both directions, the same 10 t lower cut-off for a block mass was used consistently. The amount of key blocks was best fitted with a log-normal probability density function with the expected mean M_N=125 and the standard deviation δ_N=16 (Fig. 10).

While there were no significant differences in probability density functions for the amount of blocks in the N–S and E–W tunnels, the predictions regarding block weights showed more variation. On average, the predicted block weights for the E–W tunnel had a mean of 307 t and standard deviation of 977 t, although the best-fit theoretical density function was log-normal (Fig. 11).

Discussion

The study attempted to predict the number and size of potential key blocks for the CLAB-2 tunnel by using a discrete fracture network model inferred from very limited data.

Geological/structural homogeneity

The geological homogeneity at the CLAB site was assessed by the non-parametric null hypothesis tests with fracture intensity as the test parameter. The fact that the H_0 tests failed for boreholes D6-D3 and for D2-D8 could mean that the fracture intensities within these two groups did not belong to the same statistical population. It could, be possible however, that the fracture intensities from D6 or D2 belonged to the same population as the fracture intensities found within the group D1-D4-D7. The different orientation of the boreholes, however, meant this could not be confirmed. The rejection of the null hypothesis test might also be due to the existence of undetected weakness zones intersecting one borehole but not the other. Consequently, one borehole might include fracture clusters of high intensity forming rather distinct deterministic structures, while the other could have only "background" fracturing, i.e. fractures considered as crucial for the stochastic network.

Caution must also be exercised when considering data sets obtained from different measurement methods. The acceptance of the null hypothesis for the K-S test on boreholes KSI31 (borehole camera fracture data) and D5 (direct core observations) could be attributed to spatial homogeneity of fracture intensities within the area embracing both boreholes (Table 3). On the other hand, the rejection of the null hypothesis in such a case does not necessarily mean that the fractures belong to two different populations.

It is not possible to provide a complete list of conditions that have to be fulfilled in order to obtain reliable results when performing statistical null hypothesis tests. Nevertheless, with the support from the homogeneity study of fracture intensities at the CLAB site, it is considered that the greatest reliability from testing will be obtained when:

1. Fracture data are derived using the same detection method,
2. Tested data are taken from boreholes with the same orientation and diameter,
3. Fractures are corrected for orientation sampling bias,
4. Fractures belonging to weakness zones are discarded.

The population tests using M-W and K-W procedures were performed with 5% significance level and for K-S methods, 10% significance level. There are no strict rules as to the choice of significance level. In some circumstances it might be advisable to decrease the significance level, e.g. where there are no data from outcrop mapping and/or seismic survey and consequently any speculation of the presence of different tectonic/lithological units would

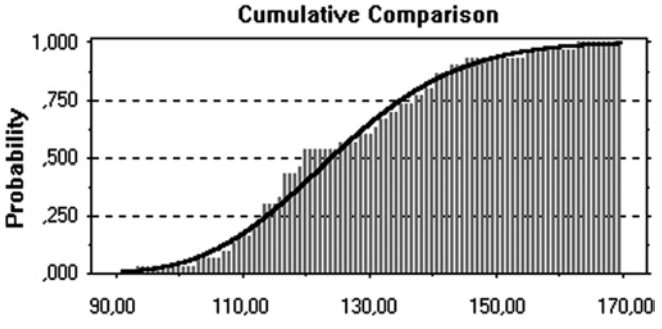

Fig. 10.
Simulated number of key blocks (vertical bars) and the best-fit pdf (thick line) for the E–W tunnel. Population mean M_N=125, population standard deviation δ_N=16

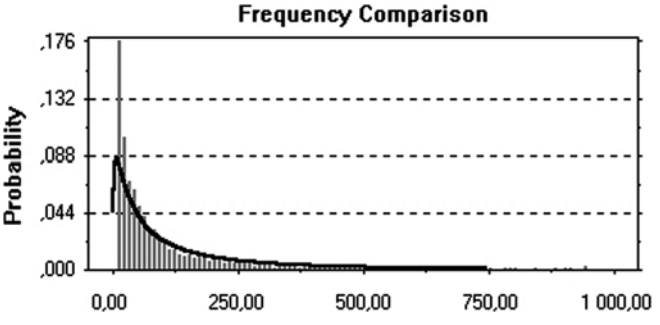

Fig. 11.
Simulated block weights (vertical bars) and the best-fit log-normal pdf (thick line) for the E–W tunnel. Population mean M_W=307 t, population standard deviation δ_W=977 t

be very tentative. In such a case it may be decided to make the population tests more robust, i.e. less sensitive to spatial variability of fracture intensities, and to decrease the significance level of the test. By so doing, the influence of undetected but theoretically existing fracture zones on the structural/geological homogeneity is reduced.

Uncertainties of the DFN model

The discrete fracture network model for the CLAB site summarized in Table 5 is the product of a stochastic generation process and as such relies on many assumptions, each having its own uncertainty. The accuracy of the final block analysis depends on the validity of the fracture network model. The main sources of errors influencing the reliability of the DFN model are: conceptual uncertainty, the accuracy and precision of field measurements and statistical uncertainty due to deviations of the theoretical probability distributions from the observed data. In this work no attempt was made to treat the uncertainty issue in detail, but the model sensitivity analysis is worth considering in further studies. The conceptual model of the CLAB site was derived from the interpretation of the geology at the site, refraction seismics and borehole measurements.

Validation of the DFN model

Validation of the DFN model was one of the crucial aspects in evaluating the appropriateness of the generated stochastic fracture network. Albeit the applied computer code allows very sophisticated mathematical models to be set up, the interpretation of the final product must be followed by critical verification. It would be naïve to believe that even with carefully evaluated input variables, one set of Monte Carlo simulations would provide a reliable outcome. Modelling is a trial and error process, conditioned on resetting and refining input parameters until an acceptable agreement with field observations is reached. For example, after finding the "true" P_{32}, the synthetic sampling resulted in a P_{10} higher for KSI31 than for KSI32, while the observed fracture intensities showed the contrary. This discrepancy was probably caused by applying too low a Terzhagi correction factor to reduce orientation sampling bias. As a consequence, there was insufficient compensation made for the subvertical fractures in vertical borehole KS132. To correct for this, the correction factor was increased from 5 to 6, which provided an appropriate P_{10} in KSI31 and KSI32 for the synthetic sampling and field observations. This operation did not make any substantial changes to the estimated fracture radii or the spatial fracture pattern. The new fracture orientation input data were then "bootstrapped" and incorporated in the DFN model.

Rock block analysis

The results from key block studies showed a relatively large variation both in respect of the number of blocks and their weights. This variation was mainly caused by the observed natural scatter of the input parameters for the DFN model, such as fracture radii variation (Fig. 6) or fracture orientation. Expanding the size of the DFN model and running more Monte Carlo realizations would probably make the pdf's from the block stability analysis more representative. In this study, however, it was decided to focus on demonstrating the application of the DFN model for predicting key blocks rather than embarking on a quantification of the accuracy of the predictions.

It should be pointed out that a block stability analysis for the CLAB-2 site was previously undertaken by Stille and Fredriksson (1996). They used the computer code Unwedge (developed by J. Carvalho, E. Hoek and B. Li from Rock Engineering Group, University of Toronto) and in contrast to the analysis presented in this study, they took into consideration friction along fracture planes and distribution of rock stress around the tunnel perimeter. Stille and Fredriksson derived the mass and shape of key blocks by studying ten combinations, each with three fracture orientation sets, where six orientation sets were applied in total. For each combination the potentially largest key block was found. Stille and Fredriksson found the maximum weight of key block to be about 178,000 t, which is three times larger that the outcome from this study. As their analysis was based on different constraints, however, there were considerable problems in comparing the two approaches. However, the results from the present study suggest that the DFN approach is likely to reduce the overestimation of block sizes resulting from their study as the fractures used here were of finite size and hence more realistic. However, in further studies, it would be interesting to compare the two methods using identical input fracture variables.

By relating rock block statistics for the N–S and E–W oriented tunnels, it was concluded that the differences were not very significant but sufficient to clearly link the prediction outcome with the direction of the long axes of the tunnels. The amount of unstable blocks for the N–S and E–W tunnels approximated with log-normal pdf had almost the same means (see Figs. 8 and 10). It was predicted that on the whole, a greater number of larger blocks would form around the E–W tunnel perimeter than around the N–S tunnel, as the mean of the pdf for the E–W tunnel was 307 t (Fig. 11) compared with the mean pdf of 235 t for the N–S tunnel (Fig. 9).

As an alternative to the predictions of the number of blocks and block weights inferred directly from the best-fit probability density functions, a simpler option is proposed. The number of unstable blocks within a specific weight interval found from the experimental frequency plot could be used, i.e. not approximated by any continuous statistical distribution but taken directly from block statistics. Table 6 presents the number of unstable blocks corresponding to several arbitrary weight ranges for the two tunnel directions.

The examination of the pdf's for the prediction of the number of blocks/weights for both tunnel orientations suggests that the N–S direction is possibly a better alternative than the E–W direction. Both the amount of unstable blocks larger than 1,000 t and their average weight were lower for the N–S tunnel.

Table 6.
Prediction of the number of unstable blocks within the specified weight range for N–S and E–W oriented tunnels at the CLAB site. Results were obtained directly from the experimental frequency distribution from block analysis

Block weight (10^3 kg)	Number of unstable blocks	
	N–S orientation	E–W orientation
10–50	50	48
50–200	39	38
200–1,000	25	26
>1,000	8	13

The study at the CLAB site illustrated the applicability of discrete fracture network modelling for rock block analysis. These kinds of predictions appear to have the greatest value in the early stages of an excavation project when different excavation scenarios are being considered. By testing how the orientation of the tunnel affects the block statistics, an optimal tunnel direction (and also its dimensions and shape) can be found in which the amount and size of key blocks will be minimal.
It is intended to carry out further studies to examine how additional fracture data will influence stability predictions for the CLAB-2 facility and how the block statistics respond to individual variations in the input parameters used for the DFN model generation.

Conclusions

A stochastic discrete fracture network model for the CLAB site located in crystalline basement on the southeast coast of Sweden was built. Prior to model generation a study of the geological/structural homogeneity was undertaken by carrying out null hypothesis tests on fracture intensities. Non-parametric Kolmogorov-Smirnov, Mann-Whitney and Kruskal-Wallis statistics and the moving average procedure carried out on fracture intensities from 12 boreholes provided results that supported the hypothesis of geological/structural homogeneity of the modelled rock volume. For the generation of a stochastic fracture model, fracture centres were assigned random positions, their orientations were directly "bootstrapped" from the observed field data and their size was inferred from aperture measurements and empirical relationship to the joint length.
The modelled fracture network was used for predicting the key blocks for two different orientations of the 115 m long tunnel: one actually existing – the CLAB-2 facility striking N–S – and another postulated tunnel oriented E–W. Comparison of the results for block predictions for the two tunnel directions showed small but distinct differences in probability density distributions for the amount of unstable blocks and their weights. The predictions presented may be valuable for the design of tunnel support and in decision-making on the optimal positioning of an underground cavern.

Acknowledgements This study was supported with Grant 821(621) from the Swedish Rock Engineering Research (SveBeFo). The authors thank Golder Assoc. Inc. in Seattle for permission to use the RockBlock code. Bill Dershowitz, Jan Hermanson, Nils Outters and Martin Stigsson are thanked for sharing their experience on stochastic fracture field. Paul La Pointe is thanked for his hints on fractal concept and fracture clustering and Tommy Norberg is appreciated for his advice on statistical data treatment. Swedish Nuclear Fuel and Waste Management (SKB) provided the data set and all written documentation on the CLAB site.

References

Andersson J, Dverstorp B (1987) Conditional simulations of fluid flow predictions in three dimensional networks of discrete fractures. Water Resour Res 23(10):1876–1886
Baecher GB, Lanney NA, Einstein HH (1977) Statistical description of rock properties and sampling. In: Wang FD, Clark GB (eds) Energy resources and excavation technology. Colorado School of Mines, Golden, Colorado, pp 5C1.1–5C1.8
Barton C, La Pointe P (1995) Fractals in the earth sciences. Plenum Press. New York, 265 pp
Båth M (1974) Spectral analysis in geophysics. Elsevier, Amsterdam, 563 pp
Brown SR (1995) Measuring the dimension of self-affine fractals: example of rough surfaces. In: Barton C, La Pointe P (eds) Fractals in the earth sciences. Plenum Press, New York, pp 77–87
Castaing C, Bourgine B, Chilés JP, Genter A (1998) From joint and fault quantification to simulation of 3-D conceptual fracture models. In: Rossmanith HP (ed) Mechanics of jointed and faulted rock. Proc 3rd Int Conf on Mechanics of Jointed and Faulted Rock, Vienna, 6–9 April, pp 145–149
Chilés JP (1988) Fractal and geostatistical methods for modeling of a fracture network. Math Geol 20(6):631–654
Chilés JP, de Marsily G (1993) Stochastic models of fracture systems and their use in flow and transport modeling. In: Bear J, Tsang CF, de Marsily G (eds) Flow and contaminant transport in fractured rocks. Academic Press, San Diego, pp 169–236
Davis JC (1986) Statistics and data analysis in geology. Wiley, New York, 646 pp
Dershowitz W (1984) Rock joint systems. PhD Thesis, Massachusetts Institute of Technology, Cambridge, Massachusetts
Dershowitz W, Carvalho J (1996) Key-block tunnel stability analysis using realistic fracture patterns. In: Aubertin M, Hassani F, Mitri HS (eds) Proc 2nd North American Rock Mechanics Symp NARMS '96, a regional conference of ISRM, Rock Mechanics Tools and Techniques, Publ 2, pp 1747–1751
Dershowitz W, Einstein H (1988) Characterizing rock joint geometry with joint system models. Rock Mech Rock Eng 21: 21–51
Dershowitz W, Herda H (1992) Interpretation of fracture spacing and intensity. In: Tillerson JR, Wawersik WR (eds) Rock Mechanics. Proc 33rd US Symposium, Publ 33, pp 757–766
Dershowitz W, Ushida M (1999) Äspö Hard Rock Laboratory. TRUE Block Scale project. Spatial data analysis. Rep ITD-99–30. Swedish Nuclear Fuel and Waste Management, Stockholm, 27 pp
Dershowitz W, Carvalho J, Foxford T (1995) FracMan/RockBlock. Discrete fracture rock block stability analysis. User documentation, version 1.0. Golder Assoc, Seattle, Washington
Dershowitz W, Lee G, Geier JE, Foxford T, La Pointe P, Thomas A (1998) FracMan. Interactive discrete feature data analysis, geometric modeling and exploration simulation. User documentation, version 2.6. Golder Assoc, Seattle, Washington

Efron B (1982) The Jacknife, the bootstrap, and other resampling plans. SIAM monograph no. 38. Society of Industrial and Applied Mathematics. Philadelphia, Pennsylvania, 92 pp
Ericsson LO (1987) Fracture mapping on outcrops. Rep PR 25–87–05. Swedish Nuclear Fuel and Waste Management, Stockholm
Eriksson K (1982) CLAB, Byggnadsgeologisk uppföljning av transporttunnlar och bergrum. Rep PM 95–3450–08. Swedish Nuclear Fuel and Waste Management, Stockholm
Follin S, Hermanson J (1996) A discrete fracture network model of the Äspö TBM tunnel rock mass. Rep AR D-97–001. Swedish Nuclear Fuel and Waste Management, Stockholm, 55 pp
Geier JE, Thomas AL (1996) Discrete-feature modeling of the Äspö site: discrete fracture network models for the repository scale. Rep 96:5. Swedish Nuclear Power Inspectorate, Stockholm
Geier JE, Axelsson CL, Hässler L, Benabderrahmane A (1992) Discrete fracture modeling of the Finsjön rock mass. Phase 2. Rep TR 92–07. Swedish Nuclear Fuel and Waste Management, Stockholm, 207 pp
Genter A, Traineau H, Dezayes Ch, Elsass Ph, Ledesert B, Meunier A, Villemin Th (1995) Fracture analysis and reservoir characterization of the granitic basement in the HDR Soultz project (France). Geotherm Sci Tech 4(3):189–215
Gibbons JD, Chakraborti S (1992) Nonparametric statistical inference. M. Dekker, New York, 544 pp
Goodman RE, Shi G (1985) Block theory and its application to rock engineering. Prentice Hall, Englewood Cliffs, 562 pp
Gustafsson Ch, Stråhle A (1997) Borehole TV images from KSI 31 and KSI 32. Rep PM PPM 97–3450–12. Swedish Nuclear Fuel and Waste Management, Stockholm
Herda HH, Einstein HH, Dershowitz WS (1991) Problems with representation of rock-fracture clusters. J Geotech Eng 117(11):1754–1771
Hermanson J, Stigsson M, Pringle A (1999) Äspö Hard Rock Laboratory. Prototype repository DFN Model No. 1. Rep IPR-99–09. Swedish Nuclear Fuel and Waste Management, Stockholm, 54 pp
Hoerger SF, Young DS (1990) Probabilistic prediction of keyblock occurrences. In: Hustrulid WA, Johnson GA (eds) Rock mechanics contributions and challenges. AA Balkema, Rotterdam, pp 229–236
Isaaks EH, Srivastava RM (1989) Applied geostatistics. Oxford University Press, New York, 561 pp
Jakubowski J, Tajdus A (1995) The 3D Monte-Carlo simulation of rigid blocks around a tunnel. In: Rossmanith HP (ed) Proc 2nd Int Conf on the Mechanics of Jointed and Faulted Rock. AA Balkema, Rotterdam, Publ 2, pp 551–556
La Pointe P, Wallman W, Follin S (1995) Estimation of effective block conductivities based on discrete fracture network analysis using data from the Äspö site. Rep TR 95–15. Swedish Nuclear Fuel and Waste Management, Stockholm
Mardia KV (1981) Directional statistics in geosciences. Commun Statist Theor Meth A10(15):1523–1543
Moberg M (1995a) Utbyggnad av lagringskapacitet Clab-Simpevarp. Berggrundundersökning 1978. Rep PM 95–3450–06. Swedish Nuclear Fuel and Waste Management, Stockholm
Moberg M (1995b) Utbyggnad av lagringskapacitet Clab-Simpevarp. Berggrundundersökning 1979. Rep PM 95–3450–07. Swedish Nuclear Fuel and Waste Management, Stockholm
Priest SD (1993) Discontinuity analysis for rock engineering. Chapman and Hall, London, 473 pp
Priest SD, Hudson JA (1976) Discontinuity spacings in rock. Int J Rock Mech Min Sci Geomech Abstr 13:135–148
Shapiro A, Delport JL (1991) Statistical analysis of jointed rock data. Int J Rock Mech Min Sci Geomech Abstr 28(5):375–382
Stanfors R, Rhén I, Larsson H (1995) Utbyggnad av lagringskapacitet. Berggrundundersökningar 1995. Rep PR 95–13. Swedish Nuclear Fuel and Waste Management, Stockholm, 31 pp
Stille H, Fredriksson A (1996) CLAB-Etapp 2. Bergmekanisk utredning av stabilitetsförhållanden och inverkan på befintligt bergrum. Rep PR 96–06. Swedish Nuclear Fuel and Waste Management, Stockholm, 26 pp
Swan ARH, Sandilands M (1995) Introduction to geological data analysis. Blackwell Science, London, 446 pp
Terzhagi RD (1965) Sources of errors in joint surveys. Geotechnique 15:287–304
Turcotte DL, Huang J (1995) Fractal distributions in geology, scale invariance, and deterministic chaos. In: Barton C, La Pointe P (eds) Fractals in the earth sciences. Plenum Press, New York, pp 1–40
Wallis PF, King MS (1980) Discontinuity spacings in crystalline rock. Int J Rock Mech Min Sci Geomech Abstr 17:63–66
Vermilye JM, Scholz ChH (1995) Relation between vein length and aperture. J Struct Geol 17(3):423–434
Warburton PM (1980) Stereological interpretation of joint trace data. Int J Rock Mech Min Sci Geomech Abstr 17:181–190
Warburton PM (1981) Vector stability analysis of an arbitrary polyhedral rock block with any number of free faces. Int J Rock Mech Min Sci Geomech Abstr 18:415–427